On the incidence rate of RR Lyrae stars with non-radial modes

H. Netzel[1,2,3], V. Varga[1,4], R. Szabó[1,2,4], R. Smolec[5], and E. Plachy[1,2,4]

[1] Konkoly Observatory, HUN-REN Research Centre for Astronomy and Earth Sciences, MTA Centre of Excellence, Konkoly-Thege Miklós út 15-17, H-1121, Budapest, Hungary
[2] MTA CSFK Lendület Near-Field Cosmology Research Group, H-1121 Konkoly Thege Miklós út 15-17, Budapest, Hungary
[3] Institute of Physics, Laboratory of Astrophysics, École Polytechnique Fédérale de Lausanne (EPFL), Observatoire de Sauverny, 1290 Versoix, Switzerland
[4] ELTE Eötvös Loránd University, Institute of Physics and Astronomy, 1117, Pázmány Péter sétány 1/A, Budapest, Hungary
[5] Nicolaus Copernicus Astronomical Center, Bartycka 18, 00-716 Warsaw, Poland

ABSTRACT

Context. Over the recent years, additional low-amplitude non-radial modes were detected in many of the first-overtone RR Lyrae stars. These non-radial modes form a characteristic period ratio with the dominant first-overtone mode of around 0.61. The incidence rate of this phenomenon changes from population to population. It is also strongly dependent on the quality of the analyzed data. Current models explaining these additional signals involve non-radial modes of degrees 8 and 9.

Aims. Using synthetic horizontal branch populations, we investigate the incidence rate of first-overtone RR Lyrae stars with non-radial modes depending on the population properties, i.e., ages and metallicities. We compare our results with the observed results for globular clusters and the numerous collection of field first-overtone RR Lyrae stars to test the predictions of the models.

Methods. We used synthetic horizontal branches combined with pulsation models to predict how the incidence rate would depend on the age and metallicity of the population. To test whether the results based on synthetic horizontal branches are realistic, we compared them to incidence rates observed by TESS in first-overtone field RR Lyrae stars, using photometric metallicity values from a newly established calibration for TESS.

Results. The analysis of synthetic horizontal branches showed that the incidence rate decreases with decreasing metallicity. We inferred photometric metallicity for RR Lyrae stars observed by TESS and showed that the theoretical predictions are in agreement with the observations. Using the same method, we also conclude that the metallicity distribution of RR Lyrae stars showing an additional mode with a period-ratio around 0.68 appears to be different from that of both all first-overtone stars and those showing additional non-radial modes.

Key words. Stars: variables: RR Lyrae – Stars: oscillations (including pulsations) – Stars: horizontal-branch

1. Introduction

RR Lyrae stars are low-mass population II pulsating stars located at the intersection of the horizontal branch (HB) with the classical instability strip. The majority of them pulsate typically in radial fundamental mode (RRab type) or first overtone (RRc type). Double-mode pulsations fundamental mode and first overtone (RRd type) are also often observed among RR Lyrae stars. Double-mode pulsations in the fundamental mode and the second overtone are also known but are rare (see e.g. Benkő et al. 2010). Six RR Lyrae stars were reported as possible triple-mode pulsators in radial fundamental mode, first overtone and second overtone (Jurcsik et al. 2015; Soszyński et al. 2019).

Besides the dominant pulsations in radial modes, many more phenomena are currently known to occur in RR Lyrae stars. The long-standing mystery is the Blazhko effect, which is a quasi-periodic modulation of the amplitude and/or phase of pulsations. It was discovered more than a hundred years ago by Blažko (1907). The Blazhko effect is more common among RRab stars (around 50 per cent, e.g. Jurcsik et al. 2014) than among RRc stars (around 10 per cent, see Netzel et al. 2018). The modulation in RRd stars was also reported, typically in anomalous RRd stars (aRRd, see e.g. Soszyński et al. 2016, and references therein).

Another phenomenon observed in RR Lyrae stars is the presence of additional signals that cannot correspond to radial modes. Multiple groups of stars with such additional signals were reported already (for a review see Netzel 2023). The so-called $RR_{0.61}$ stars are the most common group. These are originally classified as either RRc or RRd stars in which the additional low-amplitude short-period signal forms a period ratio of around 0.60–0.64 with the first overtone. A characteristic feature of this group is that these stars form three sequences in the Petersen diagram, i.e., a diagram of period ratio vs longer period (see e.g. fig. 1 in Smolec et al. 2017a). The three sequences are at the period ratio of around 0.61, 0.62, and 0.63. Henceforth, throughout this paper, we will use f_{61}, f_{62}, f_{63} while describing individual signals falling into one of these sequences. Currently, more than a thousand $RR_{0.61}$ stars are known, the majority of which were detected with the ground-based Optical Gravitational Lensing Experiment (Netzel & Smolec 2019), but also numerous sample was found only recently in the space-based missions TESS (Benkő et al. 2023) and K2 (Netzel et al. 2023). Additionally, many of the $RR_{0.61}$ stars were detected during studies of smaller samples (e.g. Jurcsik et al. 2015; Smolec et al. 2017b; Moskalik et al. 2015; Forró et al. 2022; Molnár et al. 2023, and references therein). The explanation of these additional signals was proposed by Dziembowski (2016), who suggested that they are caused by harmonics of non-radial modes of degrees $\ell = 8, 9$, where harmonic of the non-radial mode of degree 8 corresponds

to the f_{63} signals, and of degree 9 corresponds to the f_{61} signals. The f_{62} is a linear combination of the two non-radial modes. We note that similar signals to those in $RR_{0.61}$ stars were detected in classical Cepheids as well (e.g. Soszyński et al. 2008; Smolec & Śniegowska 2016; Süveges & Anderson 2018; Rathour et al. 2021; Smolec et al. 2023, and references therein). The model by Dziembowski (2016) predicts that the additional signals in classical Cepheids are caused by harmonics of non-radial modes of degrees $\ell = 7, 8, 9$. Interestingly, a similar signal was detected in one anomalous Cepheid only recently by Plachy et al. (2021).

Another interesting multi-mode group of RR Lyrae stars is the so-called $RR_{0.68}$ (Netzel et al. 2015a). These are RRc in which the additional signal, f_{68}, has a period longer than the first-overtone and forms a period ratio of around 0.686. Since the first detection more and more $RR_{0.68}$ stars are identified in various stellar systems (e.g. Netzel & Smolec 2019; Molnár et al. 2022; Benkő et al. 2023). Again, the analogous multi-mode group was also identified among classical Cepheids (Süveges & Anderson 2018; Smolec et al. 2023). The only explanation for f_{68} signals was proposed by Dziembowski (2016), but it faces several difficulties (see a discussion in Sec. 4). Only recently, Benkő & Kovács (2023) reported discovery of analogous signals in RRab stars.

The incidence rates of $RR_{0.61}$ stars are different depending on the studied sample. The dominant factor influencing the incidence rates is the quality of photometry. Netzel & Smolec (2019) analyzed RRc stars based on the OGLE-IV data for the Galactic bulge fields and obtained an incidence rate of 8.3 per cent for $RR_{0.61}$ stars. On the other hand, Netzel et al. (2015c) analyzed only the two most frequently sampled Galactic bulge fields from the OGLE-IV data and obtained a significantly higher incidence rate of 27 per cent. As expected, using space-based data typically results in a higher incidence rate than using ground-based photometry. From the ground-based data, the incidence rate does not exceed 60 per cent, except for the NGC 6362 study, where the incidence rate of the $RR_{0.61}$ stars is as high as 62.5 per cent of the RRc sample (Smolec et al. 2017b). From the space-based data, the incidence rate usually exceeds 60 per cent. In this regard, a record holder is the stars from the original *Kepler* field, where the inferred incidence rate reaches 100 per cent (Moskalik et al. 2015; Forró et al. 2022). The literature incidence rates of the $RR_{0.61}$ stars from different stellar systems and based on various studies are collected in Table 1. An interesting result from color-magnitude diagrams is that $RR_{0.61}$ stars tend to avoid the bluest region of it (Jurcsik et al. 2015; Smolec et al. 2017b; Molnár et al. 2022). Netzel & Smolec (2022) calculated a grid of theoretical models of RR Lyrae stars pulsating in radial and non-radial modes of degrees predicted by Dziembowski (2016) and showed that close to the blue edge of the instability strip, these non-radial modes are linearly stable. Consequently, in stellar systems with densely populated horizontal branches, the incidence rate of $RR_{0.61}$ is expected to be lower than 100 per cent due to the lack of excitation of those non-radial modes in the stars close to the blue edge of the instability strip.

Incidence rate is not the only difference between $RR_{0.61}$ stars from different studies. There are also differences in the Petersen diagram between different samples of $RR_{0.61}$ stars (see a discussion in Molnár et al. 2022, and their fig. 13). The scatter, appearance of characteristic sequences, and average period ratio change from sample to sample. At least some differences between the different samples of the $RR_{0.61}$ stars can be explained by differences in physical parameters, metallicities, and ages. The dependency of radial modes content on those parameters has already been studied from both observational and theoretical perspec-

tives. The occurrence of double-mode RR Lyrae stars in different stellar systems was studied recently by Braga et al. (2022), who reported that the fraction of RRd stars to all RR Lyrae stars increases with decreasing metallicity of the system. Zhang et al. (2022) reported that the ratio of fundamental to first-overtone classical Cepheids increases with increasing average population metallicity. The mode selection was studied from a theoretical perspective by Szabó et al. (2004) in the context of double-mode RRd stars (see, however, a discussion in Smolec & Moskalik 2008 on problems with modeling double-mode RR Lyrae stars).

In this work, we aim to characterize the incidence rate of $RR_{0.61}$ stars, assuming that the signals in these stars are indeed explained by non-radial modes of degrees 8 and 9. First, we calculated synthetic horizontal branches using horizontal branch evolutionary tracks. Then, we used pulsation models to determine how many stars in the horizontal branch would be RRc stars and how many of those would also have non-radial modes of degree 8 or 9 unstable. We varied age and metallicity when calculating synthetic horizontal branches. Based on those results, we can predict the incidence rate of $RR_{0.61}$ stars for different metallicities and ages. We tested our results by comparing them with the numerous sample of field RRc stars observed within the TESS project and analyzed by Benkő et al. (2023) and to a few globular clusters which were already analyzed in the literature and have derived observed incidence rates of the $RR_{0.61}$ stars.

Additionally, we present a distribution of photometric metallicity for $RR_{0.68}$ stars based on the numerous sample identified by Benkő et al. (2023) in the TESS data.

The paper is structured as follows. Methods are presented in Sec. 2. The results are described in Sec. 3 and discussed in Sec. 4. Sec. 5 summarizes our findings.

2. Methods

2.1. Synthetic horizontal branches

We followed the method from Lee et al. (1990) to create synthetic horizontal branches for a given age and metallicity. The masses are drawn randomly from the truncated Gaussian distribution:

$$P(M) = [M - (\langle M_{HB} \rangle - \Delta M)] \, (M_{RG} - M) \exp\left[-\frac{(\langle M_{HB} \rangle - M)^2}{\sigma_M^2}\right],$$
(1)

where M is the mass of each horizontal branch star, $\langle M_{HB} \rangle$ is a mean mass of stars on the horizontal branch, M_{RG} is a mass of a star on the tip of the red giant branch if no mass loss occurred, ΔM is mass lost on average, i.e. $\Delta M = M_{RG} - \langle M_{HB} \rangle$, and σ_M is a mass dispersion. We assumed that stars arrive at the horizontal branch at a constant rate regardless of mass, i.e. the age is drawn randomly from a uniform distribution. We chose four values of M_{RG}: $0.80 \, M_\odot$, $0.83 \, M_\odot$, $0.85 \, M_\odot$, and $0.88 \, M_\odot$. The M_{RG} value translates to age. That is, the higher the mass, M_{RG}, the younger the system. For $Z \approx 0.001$ these masses correspond to the ages of around 13.7, 12, 11, and 9.7 Gyr, respectively. For lower metallicities, $Z \approx 0.0003$, thses masses correspond to the ages of around 12.5, 11, 10, and 9 Gyr.

We used solar-scaled horizontal branch tracks from the BaSTI database (Pietrinferni et al. 2004). From the available tracks, we chose four sets of tracks for the following metal and helium abundances (Z, Y): (0.0001, 0.245), (0.0003, 0.245), (0.0006, 0.246), and (0.001, 0.246). These values were chosen

| System	Incidence rate	$N_{RR_{0.61}}$	Reference
Galactic bulge (OGLE-III)	5.6%	145	Netzel et al. (2015b)
Galactic bulge (2 fields of OGLE-IV)	27%	131	Netzel et al. (2015c)
Galactic bulge (OGLE-IV)	8.3%	949	Netzel & Smolec (2019)
Pisces K2	75%	3	Molnár et al. (2015)
TESS (first-light results)	65%	20	Molnár et al. (2022)
TESS	72%	456	Benkő et al. (2023)
Kepler field	100%	4	Moskalik et al. (2015)
Kepler field (*Kepler* Pixel Project)	100%	6	Forró et al. (2022)
K2	62%	452	Netzel et al. (2023)
M80 (K2)	62.5%	5	Molnár et al. (2023)
NGC 5897 (K2)	11%	1	Kalup et al. (in prep.)
M3	38%	14	Jurcsik et al. (2015)
NGC 6362	63%	10	Smolec et al. (2017b)

Table 1. Incidence rates of $RR_{0.61}$ stars from the literature. Consecutive columns provide the stellar system (and the particular study), derived incidence rate, the total number of identified $RR_{0.61}$ stars and the reference for the study.

arbitrarily to cover the metallicity range of RR Lyrae stars and correspond to [M/H]=−2.267, [M/H]= −1.790, [M/H]= −1.488, and [M/H]= −1.266, respectively. For each value of mass, M_{RG}, and metallicity, we interpolated between the evolutionary tracks using linear interpolation to obtain the synthetic horizontal branch population. Each horizontal branch was populated with 500 stars. We adopted $\sigma_M = 0.02$ to be constant. We also set $\Delta M = 0.15$. We note that in the literature both values are varied. Average mass loss can also be connected to metallicity. In this analysis, however, we did not study those nuances. The principal goal is to study main trends, not to reproduce a particular globular cluster exactly. We also repeated the same analysis using α−enhanced tracks from the BaSTI database and the results do not change the conclusion drawn from the analysis of solar-scaled tracks.

In Fig. 1 we plotted simulated horizontal branch stars for different M_{RG} and two values of metal abundance: $Z = 0.001$ (top panel) and $Z = 0.0001$ (bottom panel). The population is shifting towards lower effective temperatures for higher M_{RG}. For the same M_{RG}, the population is shifted towards lower temperatures for higher Z. In the case of $Z = 0.001$, the population corresponding to $M_{RG} = 0.88 M_\odot$ is outside the instability strip. In the case of $Z = 0.0001$, the population corresponding to the lowest considered mass, $M_{RG} = 0.80 M_\odot$, is located outside of the instability strip.

In Fig. 2 we plotted synthetic HB stars for different metal abundances Z, and two different M_{RG}: 0.80 (top panel) and 0.88 $M_\odot$ (bottom panel). First, for lower mass, $M_{RG} = 0.8 M_\odot$, the scatter on the HR diagram is larger. The effect of metal abundance is clearly visible. Namely, the higher the metallicity, the more towards the lower effective temperature is the population shifted. Consequently, inside the instability strip, the stars are shifted towards lower luminosities with increasing metallicity forming a known absolute brightness – metallicity relation, M_V−[Fe/H] (e.g. Fernley et al. 1998). As already visible from Fig. 1, for the lowest mass and lowest metallicity, the population is located outside the instability strip. The same situation is for the highest mass and the highest metal abundance.

We note that in Figures 1 and 2 the instability strip edges are plotted based on Marconi et al. (2015), who provides a position of the fundamental red edge and first-overtone blue edge. However, to select first-overtone RR Lyrae stars from the synthetic populations, it is necessary to know the position of the first-overtone red edge. Therefore, we calculated blue and red
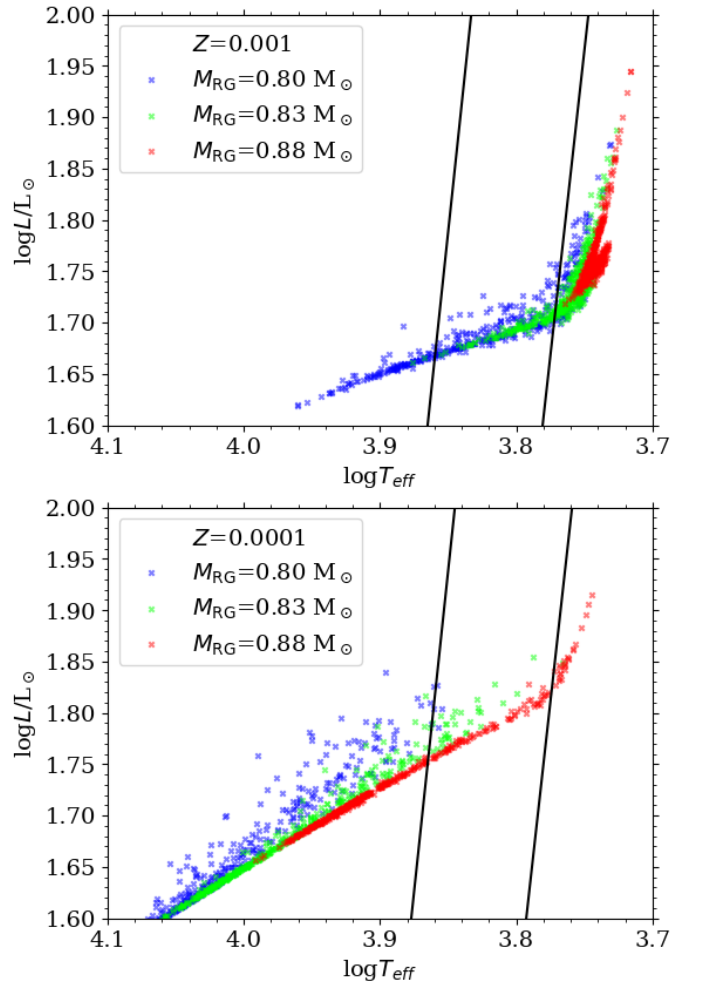
Fig. 1. Synthetic horizontal branch stars on the Hertzsprung–Russell diagram. The mass at the tip of the RGB is color-coded as indicated in the key. Black lines are instability strip edges from Marconi et al. (2015). Top panel: for $Z = 0.001$. Bottom panel: for $Z = 0.0001$.

edge for the first-overtone pulsations using envelope pulsation code MESA–RSP (Paxton et al. 2019). We calculated a grid of models for each value of metal and helium abundance matching the values of the evolutionary tracks. For each grid we chose one
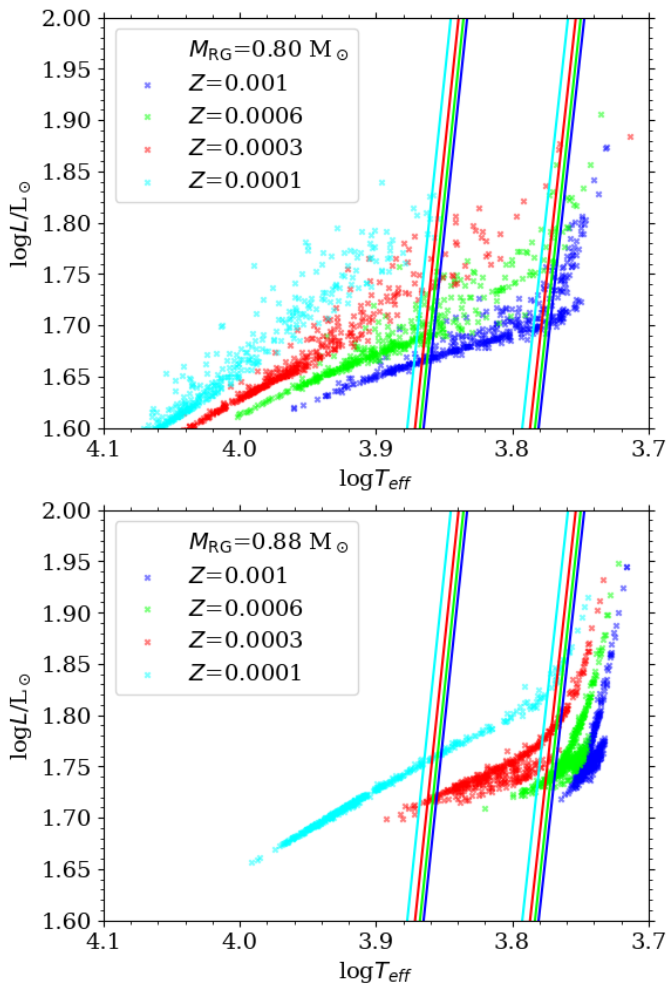
Fig. 2. Synthetic horizontal branch stars on the Hertzsprung–Russell diagram. Metal abundance Z is color-coded as indicated in the key. Instability strip edges from Marconi et al. (2015) are plotted with lines whose color also corresponds to Z. Top panel: for $M_{RG} = 0.80\,M_\odot$. Bottom panel: for $M_{RG} = 0.88\,M_\odot$.

value of mass based on mass–metallicity relation from Castellani et al. (1991). For $Z = 0.0001$ we set $M = 0.74\,M_\odot$, for $Z = 0.0003$ we set $M = 0.70\,M_\odot$, for $Z = 0.0006$ we set $M = 0.67\,M_\odot$, and for $Z = 0.001$ we set $M = 0.65\,M_\odot$. We used $\alpha_{MLT} = 1.5$ and convective parameters from set A in Paxton et al. (2019). The grid was calculated for three values of luminosity $\log L/L_\odot \in (1.5, 1.6, 1.7)$, and for effective temperature from $T_{eff} = 5700\,K$ to $8000\,K$ with a step of $100\,K$. Linear calculations were carried out and based on the linear growth rates the positions of the edges were interpolated for each metallicity.

2.2. Incidence rate based on synthetic horizontal branches

In order to estimate the incidence rate of RRc stars with non-radial modes of degrees 8 or 9, we used the grid of models already calculated by Netzel & Smolec (2022). The models were calculated using the envelope code by Dziembowski (1977) and are discussed in detail in Netzel & Smolec (2022). Here we briefly provide the most important information. The mass range covered by the grid is $0.5 - 0.9\,M_\odot$ with a step of $0.01\,M_\odot$. The metallicity range is from –3.0 dex to +0.1 dex with a 0.05 dex step. The luminosity, $\log L/L_\odot$, range is 1.3 to 1.8 dex with a step of 0.01 dex, and effective temperature, $\log T_{eff}$, range is from

3.75 to 3.91 dex with a step of 0.005 dex. The number of all models in the grid is over two million. For the further study, we selected four subgrids of models with matching Z. On average, each subgrid has around 33 000 models with linearly unstable first-overtone, and around 15 000 and 20 000 were non-radial modes of degrees 8 and 9 are unstable, respectively. We note, that the used envelope code cannot calculate the position of the red edge of the first-overtone instability strip due to the frozen-in approximation of convection. We used the calculated edges described in Sec. 2.1. We also note that the used edges are linear, while more realistic nonlinear red edge for the first-overtone is hotter.

The method to derive the incidence rate based on synthetic horizontal branch and pulsation models is presented in Fig. 3. Simulated stars on the synthetic horizontal branch are plotted with crosses. The models located in the grey area have at least one non-radial mode linearly unstable. First-overtone red edge is plotted with a red solid line, while blue edge is plotted with a blue solid line. For a given metallicity, we compared the positions of the synthetic horizontal-branch population with selected regions of instability strip provided by theoretical models. In Fig. 3 the synthetic population is plotted with black if it is outside the instability strip. In green, we plotted those stars that should be RRc stars with additional non-radial modes. Pure RRc stars are plotted with orange. In order to estimate the incidence rate together with its error, we simulated 20 HB populations for a given metallicity and M_{RG}. We counted the number of RRc stars with additional non-radial modes and all RRc stars in each simulation and the resulting incidence rate is an average from incidence rates from 20 simulations. The errors were estimated through the bootstrap resampling technique, employing a confidence level of 95 per cent based on percentiles.

2.3. Metallicity observations

For testing further if the models trying to explain the extra signals in RRc light curves with high-order non-radial modes are correct, a comparison of the synthetic and the observed metallicity dependencies of incidence rates provides a great opportunity.

For a thorough analysis, good-quality light curves are needed to detect the extra signals in as many cases as possible. In this work, we used TESS photometric measurements processed by Benkő et al. (2023). This provides us with 1357 time series analyzed in total for 670 stars brighter than 14 mag, from which 23 blended and 14 non-RRc stars were omitted leaving 633 stars for the further analysis. Note that the higher number of time series stems from the fact that some of the stars were observed during multiple TESS sectors.

Spectroscopic metallicities are not available for most of these stars. However, metallicity may be estimated in an empirical way, based on light curve shape and pulsation period. For RRc stars, the formulae were first established by Morgan et al. (2007). The hence-derived photometric metallicities are much less precise than those determined by high-resolution spectroscopy, but for a not individual but statistical purpose, as in our case, such approach is sufficient. A difficulty in the photometric metallicity estimations is, however, that the shape of the light curve varies with optical filters, and therefore the calibration of the relation has to be done separately for different passbands. Lacking a fit for TESS, we have established a new calibration for the RRc subtype. Here we present only the key aspects, details are to be found in Varga et al. (in prep.).

As the photometric calibration dataset, the same set as that for the extra signal detection (Benkő et al. 2023) was used, while

spectroscopic metallicities were provided by the Carnegie RR Lyrae Survey (CARRS, Kollmeier et al. 2013; Sneden et al. 2018). The cross-matched calibration sample consisted of 96 stars. To describe the light curve, the P_{1O} first-overtone period and the $\varphi_{31} \equiv \varphi_3 - 3\varphi_1$ Fourier phase difference were used, along with [Fe/H] indices describing the metallicity. Benkő et al. (2023) provide this value for 632 out of 633 stars. For the empirical relation, we ended up using a second-degree polynomial in the following form and getting the following values of the 4 fitting parameters:

$$[\text{Fe/H}] = -0.26 \cdot \varphi_{31}^2 - 11.5 \cdot P_{1O} + 0.96 \cdot \varphi_{31} + 2.05. \quad (2)$$

The fitting process did not consider the varying confidence in the data points of the calibration sample, hence the fitting parameters should be considered preliminary, and their final values are yet to be published in Varga et al. (in prep.). The spectroscopic metallicity values of the calibration sample range from -2.7 dex to -0.3 dex, and the root mean square deviation (RMSD) of the fit is 0.23 dex. Using such established relation for the Benkő et al. (2023) TESS sample, an [Fe/H] value was provided for all 632 stars with known φ_{31} values.

Conversion to total Z metallicities is not a straightforward procedure. Kollmeier et al. (2013) report that CARRS abundance measurements were performed by fitting to a grid of synthetic spectra generated by MOOG, for which the atomic line lists begun with the Kurucz (2011) line database, followed by further refinements. Kurucz (2011) uses the solar abundances of Anders & Grevesse (1989), who are reportedly (Grevesse et al. 2013) overestimated. Hence, despite not being the solar reference used for the abundance measurements, we can obtain presumably more accurate Z values calculating with the total solar metallicity value $Z_\odot = 0.0134$ of Asplund et al. (2009), approximating the iron contents and total metallicities to be proportional, therefore using the formula

$$Z = Z_\odot \cdot 10^{[\text{Fe/H}]}. \quad (3)$$

We note that in case of using a higher solar metallicity reference, like that of Anders & Grevesse (1989), the observed trends and therefore conclusions remain the same.

3. Results

3.1. Theoretical incidence rate

Using synthetic horizontal branches for four values of metal abundance, Z, and four values of mass at the tip of the red giant branch, M_{RG}, we were able to determine the incidence rates for different populations. These results are collected in Table. 2, and presented in Fig. 4. We note, that one population is not plotted. In the case of $M_{RG} = 0.88\,\text{M}_\odot$ and $Z = 0.001$, i.e. young and metal-rich population, there were no stars inside the instability strip, as the population was redder than the red edge (compare with Fig. 2).

There are two trends visible in Fig. 4. The incidence rate of the $RR_{0.61}$ stars depends on both metallicity and M_{RG} of the given population. The incidence rate decreases with decreasing metallicity. Moreover, typically, the incidence rate is lower for lower values of M_{RG}, which corresponds to older populations. The lowest (non-zero) values of incidence rate are reached by the population of $Z = 0.0001$ and $M_{RG} = 0.83\,\text{M}_\odot$, and the highest is for $Z = 0.001$ and $M_{RG} = 0.85\,\text{M}_\odot$, and for $Z = 0.0006$ and $M_{RG} = 0.88\,\text{M}_\odot$.
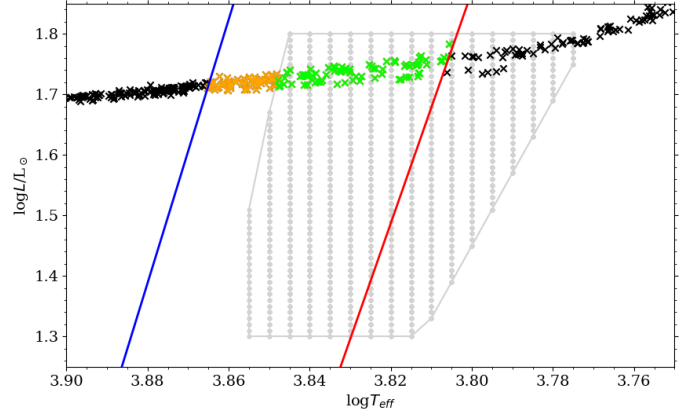
Fig. 3. Example of synthetic horizontal branch together with pulsation models used for incidence rate estimation. The models plotted with gray were calculated with the MESA–RSP code by Paxton et al. (2019). In these models, at least one non-radial mode is unstable. The red and blue line correspond to the red and blue edge for first-overtone pulsations. Synthetic horizontal branch stars are plotted with black crosses when they are outside of the instability strip, in orange if they have unstable first-overtone but stable non-radial modes, and in green when first overtone and non-radial modes are unstable.

Z	IR	IR_{min}	IR_{max}
0.80 $M_\odot$			
0.001	0.79664	0.78409	0.80882
0.0006	0.65485	0.63453	0.67332
0.0003	0.5525	0.52515	0.58045
0.0001	0	0	0
0.83 $M_\odot$			
0.001	0.91642	0.88579	0.94607
0.0006	0.81013	0.79762	0.8226
0.0003	0.6091	0.58558	0.63313
0.0001	0.28059	0.24483	0.31418
0.85 $M_\odot$			
0.001	1	1	1
0.0006	0.9104	0.89128	0.92789
0.0003	0.57177	0.55852	0.58548
0.0001	0.49106	0.45882	0.52212
0.88 $M_\odot$			
0.001	–	–	–
0.0006	1	1	1
0.0003	0.85568	0.84479	0.86656
0.0001	0.67526	0.65092	0.70054

Table 2. Theoretical incidence rates. For four different M_{RG} and Z, the columns provide the incidence rate (IR) from 20 simulations together with minimum and maximum values of IR corresponding to confidence level of 95 per cent.

3.2. Metallicity of RR Lyrae stars with additional signals

We determined photometric metallicity for RRc stars studied by Benkő et al. (2023). The distribution of metallicities is plotted in Fig. 5 for all RRc stars, and for RRc stars that were identified by Benkő et al. (2023) to show additional signals as indicated in the key.

The majority of RRc stars in Fig. 5 have metallicity from -2.0 dex to -1.0 dex. However, there are stars that have metallicity as low as -3.5 dex and as high as 0.0 dex. Stars classified as $RR_{0.61}$ or with f_{61} or f_{63} signals have metallicity distribu-
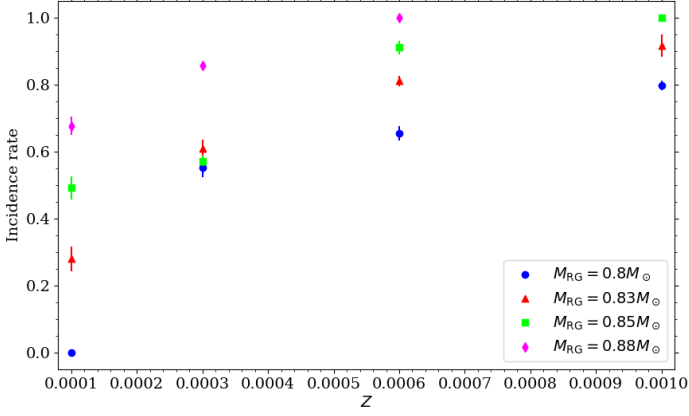
Fig. 4. Incidence rate of RR$_{0.61}$ stars as a function of metal abundance, Z. The incidence rate is calculated based on synthetic horizontal branches and pulsation models (see text for details). Different colors and symbols correspond to different masses on the tip of the red giant branch as indicated in the key.

tions that do not show large-scale differences compared to the distribution of all RRc stars. Interestingly, stars with f_{68} have a distribution that differs from the distribution of all RRc stars. Typically the RR$_{0.68}$ stars have lower metallicities than all RRc stars, and RRc stars with f_{61} or f_{63} signals. The majority of the RR$_{0.68}$ have metallicity from -1.7 dex to -1.3 dex. Moreover, while RRc stars with and without f_{61} signals can reach relatively high metallicities, the RR$_{0.68}$ are not detected for metallicity above -0.5 dex. The particularly interesting stars are those classified at the same time as RR$_{0.61}$ and RR$_{0.68}$ stars, which are also included in the distribution in Fig. 5. Their metallicity distribution shows more resemblance to the one for stars with f_{68} than to RR$_{0.61}$.

3.3. Observed metallicity dependence of incidence rates

In Fig. 6 the incidence rates of RR$_{0.61}$ stars out of all RRc stars are shown, subdivided into groups defined by their more precise period-ratio, namely the f_{61} and the f_{63} signals. We converted the photometrically estimated [Fe/H] values to total Z metallicities, then calculated the incidence rates using bins from $Z = 10^{-4}$ to $Z = 10 \cdot 10^{-4}$ with a width of $\Delta Z = 10^{-4}$. The uncertainties of the incidence rates were calculated as the standard error of the sample mean.

Comparing the observed incidence rates of at least one signal (red crosses) on Fig. 6 to the simulated results on Fig. 4, suggests a resemblance in trends. Notably, both distributions indicate lower incidence rates with decreasing metallicity. However, this observation should be verified using metallicity measurements that have better accuracy than those obtained with photometric metallicity calibrations.

4. Discussion

The predicted trend of decreasing incidence rate of the RR$_{0.61}$ stars with decreasing metal abundance was compared with observed incidence rates for field stars observed with TESS in Fig. 6. The observed and predicted trends, indicating a decrease in incidence rates with decreasing Z, seem to align well, suggesting that the simulated results and the underlying theoretical background are justified. The observed values of the incidence rates corresponding to all manifestations of non-radial modes,
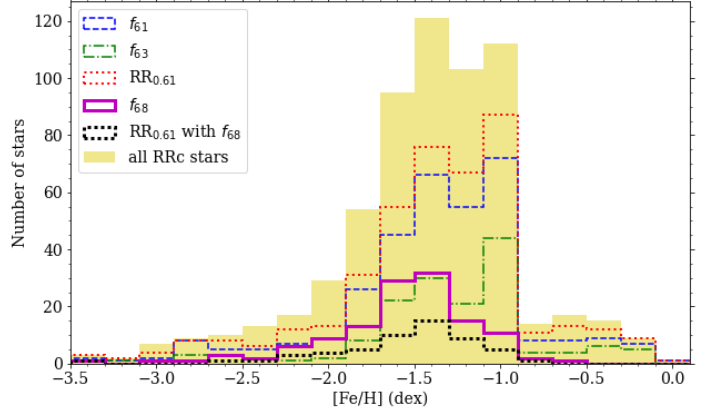
Fig. 5. Distribution of photometric metallicity for RRc stars observed by TESS and analyzed by Benkő et al. (2023). Yellow bins correspond to all RRc stars. With different line colors and types, we plotted stars that have additional signals detected as indicated in the key. The f_{61}, f_{63} and f_{68} refer to the respective signals, while RR$_{0.61}$ represents all RRc stars that show any signal that suggests the presence of the non-radial modes ($l = 8$ or $l = 9$). This means the inclusion of f_{63}, f_{61}, f_{62}, and their sub-harmonics and combinations frequencies. Note that metallicity values below -2.7 dex or above -0.3 dex are results of extrapolation, and therefore should be treated with caution.
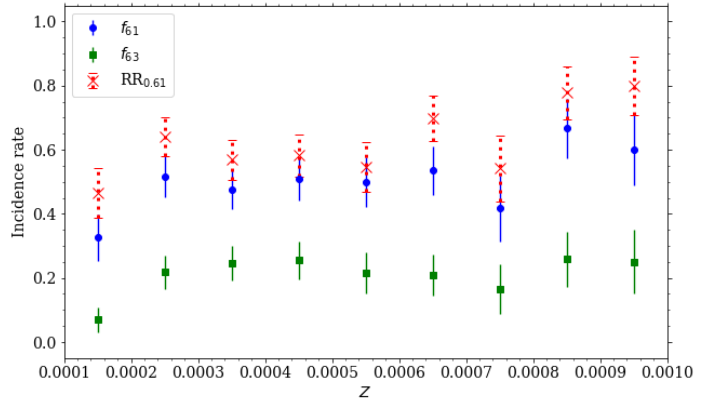
Fig. 6. Incidence rates of the f_{61} and f_{63} frequencies and of all RR$_{0.61}$ stars observed by TESS, as function of photometric metal abundance Z. The meaning of symbols in the key is the same as in Fig. 5.
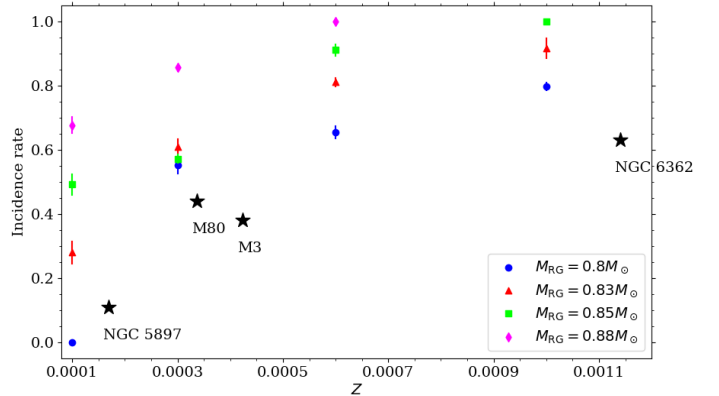
Fig. 7. The same as Fig. 4, but with four globular clusters added. They are plotted with black star symbols and their IDs are indicated in the figure.

i.e. $RR_{0.61}$ in Fig. 6, are within the range of the incidence rates based on the models. We note, the uncertainties of photometric metallicities are higher than of those determined spectroscopically. While the trend in observed photometric metallicities from the TESS sample seem to match simulated trends, this conclusion should be verified using metallicities that have smaller uncertainties.

The most uniform populations that we could compare our results to are globular clusters. Several known globular clusters were already analyzed for the occurrence of additional signals in RR Lyrae stars (see Table 1): M80, NGC 5897, M3, and NGC 6362. Interestingly, in the case of NGC 5897, which is the lowest metallicity of the above-discussed globular clusters, the incidence rate is only 11 per cent (Kalup et al. in prep.). We included these four globular clusters in Fig. 7. For M3 we adopted [Fe/H] = −1.50, for M4 – [Fe/H] = −1.18, for NGC 6362 – [Fe/H] = −1.07, and for NGC 5897 – [Fe/H] = −1.9 (Carretta et al. 2009). We used Eq. 3 to calculate Z. Interestingly, incidence rates for these four globular clusters appear to follow the same trend with metallicity, although the values of incidence rates are lower than the trend set by the models.

The caveat of the comparison between globular clusters is that they were studied using different instruments and photometric systems. M80 and NGC 5897 were observed during the K2 mission, while the observations of M3 and NGC 6362 were carried out in V band using different ground-based telescopes. These differences cause different detection limits of the $f_{0.61}$ signals and the incident rates cannot be directly compared. To estimate the impact of this problem on our analysis we consider the lowest amplitude of an additional signal detected with a given instrument as a rough estimate of its detection limit. This gives a detection limit of 0.5 mmag for M80 and NGC 5897, 5 mmag for M3, and 2.3 mmag for NGC 6362. The amplitudes of the $f_{0.61}$ signals are lower for V band than for I band by roughly a factor of two (see fig. 8 in Jurcsik et al. 2015). Since the K_p band spans approximately from I to V band, we assume that the amplitude of signals in K_p band is at most twice as large as in the V band. Even with this assumption some stars discovered in K2 would not be detected in the case of M3 and NGC 6362. Hence, the incidence rate for M3 and NGC 6362 is likely underestimated. We conclude that indeed the underlying incidence rate for M3 and NGC 6362 is likely higher than for NGC 5897 and M80.

The incidence rates observed for globular clusters seem to be lower than based on the models. There are multiple factors that might cause this difference. First, there are observational limitations. In some stars, the additional signals might have amplitudes lower than the noise level and therefore not be identified as $RR_{0.61}$. This is certainly an important factor since the observed incidence rates are strongly correlated with the quality of photometry. Moreover, distributions of amplitudes of additional signals in $RR_{0.61}$ stars show a rise in the number of stars towards low amplitudes until the cutoff due to data limitations (see e.g. figures 4 and 5 in Netzel & Smolec 2019, and fig. 11 in Benkő et al. 2023).

Second, the signals in $RR_{0.61}$ stars are not stable. Specifically, their amplitude and/or phase often vary in time. As a consequence, they form wide structures in frequency spectra, which is commonly observed (see e.g. fig. 9 in Netzel et al. 2023). With longer and more precise data it is possible to trace this variability in time. For instance, Netzel et al. (2015c) showed that frequency spectra of $RR_{0.61}$ stars can drastically change from observing season to observing season (see their fig. 10). Long-term monitoring of four RRc stars in the *Kepler* field allowed to trace these changes in more detail (see figures 6 and 7 in Moskalik

et al. 2015), which turned out to be significant. The irregularity of changes was also shown based on observations of stars in the continuous viewing zone of TESS (see figures 17 and 18 in Benkő et al. 2023). These changes might contribute to another mechanism that decreases the observed incidence rate. Namely, some $RR_{0.61}$ stars might be simply observed during phases of low amplitude of $f_{61,62,63}$ due to its non-stationary nature, and therefore not identified as $RR_{0.61}$.

The third effect that leads to decrease of the predicted incidence rate is the fact that the non-linear first-overtone red edge is hotter than the linear red edge. Therefore the number of RRc stars with unstable non-radial modes will decrease and consequently the incidence rate will be lower.

As visible from Table 2, in our simulated young and metal-rich populations there are no RR Lyrae stars. We note that there are known RR Lyrae stars with high metallicities (e.g. Liu et al. 2013), which have kinematics consistent with young thin disk (e.g. Iorio & Belokurov 2021) However, the ages of individual stars are not precisely known to verify this. Moreover, such young and metal-rich RR Lyrae stars are difficult to obtain through standard formation channel. Bobrick et al. (2024) showed that they can be created through binary evolution. To test whether young and metal-rich RR Lyrae stars population exists, we used the collection of RR Lyrae stars in galactic globular clusters prepared by Cruz Reyes et al. (2024). For metal-rich globular clusters we searched for ages in the literature and checked their population of RR Lyrae stars. Our search revealed that indeed in this sample there is no young and metal-rich globular cluster with sizeable population of RR Lyrae stars. The only candidate is Terzan 7, whose metallicity is estimated around [Fe/H] ≈ −0.6 (Harris 1996) or [Fe/H] ≈ −0.6 (Sbordone et al. 2005; Tautvaišienė et al. 2004). Its age is estimated to be 9 Gyr by Buonanno et al. (1995) or 6 Gyr by Tautvaišienė et al. (2004). However, this cluster contains only one RR Lyrae star (Cruz Reyes et al. 2024).

4.1. $RR_{0.68}$ stars

The analysis of photometric metallicities for a large sample of RRc stars from the TESS data leads to additional noteworthy results regarding the $RR_{0.68}$ stars. The metallicity of the $RR_{0.68}$ stars have a different distribution than all RRc stars, and the metallicity of the $RR_{0.68}$ stars is typically lower. We applied the Komogorov-Smirnov test to verify the difference between the two distributions. We assumed that the uncertainity of all metallicity measurements is 0.23 dex, i.e. RMSD of the fit (see Sec. 2.3). The test yielded a Kolmogorov-Smirnov statistic of 0.19 and a p-value of 0.001. With a significance level of 0.05, the null hypothesis that the two samples were drawn from the same distribution was rejected. This indicates a statistically significant difference between the distributions of the $RR_{0.68}$ and all RRc stars.

This is important in the context of explaining the nature of the $RR_{0.68}$ stars. At present, the nature of the additional signal is unknown. Dziembowski (2016) showed that the period ratio of around 0.68 can be reproduced by pulsations in radial fundamental mode and first overtone if the $RR_{0.68}$ stars are in fact not true RR Lyrae stars, but low-mass giants stripped from their envelopes similarly to binary evolution pulsator (Pietrzyński et al. 2012). This explanation, however, is challenged by stars that show $f_{61,62,63}$ and f_{68} signals simultaneously. Such stars were already detected from the ground and space-based photometry (e.g Netzel & Smolec 2019; Benkő et al. 2023; Netzel et al. 2023). Therefore explanations proposed for $RR_{0.61}$ stars and for $RR_{0.68}$

stars are mutually exclusive. We note that f_{68} signals were also detected in classical Cepheids since the development of the theory by Dziembowski (2016), and only recently in RRab stars (Benkő & Kovács 2023). So far, there was no clear observed difference between the $RR_{0.61}$ and the $RR_{0.68}$ stars. In this study, we show for the first time that in fact, the $RR_{0.61}$ and the $RR_{0.68}$ stars show differences. This observation will hopefully contribute to future efforts in explaining the nature of the additional signals in the $RR_{0.68}$ stars.

5. Conclusions

We calculated synthetic horizontal branch populations to investigate the incidence rate of stars with non-radial modes of degrees $\ell = 8, 9$. We calculated populations for four values of metallicity, (Z, Y): (0.001, 0.246), (0.0006, 0.246), (0.0003, 0.245), and (0.0001, 0.245), and for four values of mass at the tip of the red giant branch, M_{RG}: $0.80\,M_\odot$, $0.83\,M_\odot$, $0.85\,M_\odot$, and $0.88\,M_\odot$. We used BaSTI horizontal-branch evolutionary tracks (Pietrinferni et al. 2004). We used MESA-RSP code by Paxton et al. (2019) to derive the instability strip edge for first-overtone pulsations, and a grid of models from Netzel & Smolec (2022) to get the region of the instability strip where the non-radial pulsations in modes of degrees 8, and 9 occur.

We compared our theoretical predictions of incidence rates with observed incidence rates of $RR_{0.61}$ stars. We used four globular clusters with derived incidence rates: NGC 5897 (Kalup et al. in prep.), M80 (Molnár et al. 2023), M3 (Jurcsik et al. 2015), and NGC 6362 (Smolec et al. 2017b). We also used RRc stars observed by TESS and analyzed by Benkő et al. (2023). For this sample, we derived photometric metallicities based on our newly established calibration for TESS. Our findings are listed below:

- For a population with metallicity of $Z = 0.001$ and mass at the tip of the red giant branch, $M_{RG}=0.88\,M_\odot$, i.e. metal-rich and young population, all stars were outside of the instability strip. In other words, this population did not contain any RR Lyrae stars.
- For the rest of the combinations the incidence rate varied from high values, close to 100 per cent, to relatively low (non-zero) values of almost 20 per cent.
- The theoretically predicted incidence rate decreases with decreasing metallicity.
- The theoretically predicted incidence rate is lower for lower values of M_{RG}, i.e. for older populations.
- The trend of decreasing incidence rate with decreasing metallicity appear in agreement with the observed values of incidence rates for four globular clusters. The values of observed incidence rates are systematically smaller than predicted by the simulations (see a discussion in 4).
- The $RR_{0.61}$ stars from the TESS sample also show the slight trend of decreasing incidence rate with decreasing metallicity but are subject to the relatively significant error bars.

We investigated differences between metallicity distributions for the whole RRc TESS sample and stars classified as $RR_{0.61}$ or $RR_{0.68}$. The distribution of photometric metallicity for the whole RRc TESS sample and the $RR_{0.61}$ stars do not show large scale differences. Interestingly, RRc stars with the f_{68} signals show a metallicity distribution that significantly differs from the rest of the RRc sample. $RR_{0.68}$ stars tend to have typically lower metallicities. This is also the case for the $RR_{0.61}$ stars with the f_{68} signals.

References

Anders, E. & Grevesse, N. 1989, Geochim. Cosmochim. Acta, 53, 197
Asplund, M., Grevesse, N., Sauval, A. J., & Scott, P. 2009, ARA&A, 47, 481
Benkő, J. M., Kolenberg, K., Szabó, R., et al. 2010, MNRAS, 409, 1585
Benkő, J. M. & Kovács, G. B. 2023, arXiv e-prints, arXiv:2311.11670
Benkő, J. M., Plachy, E., Netzel, H., et al. 2023, Monthly Notices of the Royal Astronomical Society, 521, 443
Blažko, S. 1907, Astronomische Nachrichten, 175, 325
Bobrick, A., Iorio, G., Belokurov, V., et al. 2024, MNRAS, 527, 12196
Braga, V. F., Fiorentino, G., Bono, G., et al. 2022, MNRAS, 517, 5368
Buonanno, R., Corsi, C. E., Pulone, L., et al. 1995, AJ, 109, 663
Carretta, E., Bragaglia, A., Gratton, R., D'Orazi, V., & Lucatello, S. 2009, A&A, 508, 695
Castellani, V., Chieffi, A., & Pulone, L. 1991, ApJS, 76, 911
Cruz Reyes, M., Anderson, R. I., Johansson, L., Netzel, H., & Medaric, Z. 2024, arXiv e-prints, arXiv:2402.08843
Dziembowski, W. 1977, Acta Astron., 27, 95
Dziembowski, W. A. 2016, Commmunications of the Konkoly Observatory Hungary, 105, 23
Fernley, J., Skillen, I., Carney, B. W., Cacciari, C., & Janes, K. 1998, MNRAS, 293, L61
Forró, A., Szabó, R., Bódi, A., & Császár, K. 2022, ApJS, 260, 20
Grevesse, N., Asplund, M., Sauval, A. J., & Scott, P. 2013, in Astronomical Society of the Pacific Conference Series, Vol. 479, Progress in Physics of the Sun and Stars: A New Era in Helio- and Asteroseismology, ed. H. Shibahashi & A. E. Lynas-Gray, 481
Harris, W. E. 1996, AJ, 112, 1487
Iorio, G. & Belokurov, V. 2021, MNRAS, 502, 5686
Jurcsik, J., Smitola, P., Hajdu, G., & Nuspl, J. 2014, ApJ, 797, L3
Jurcsik, J., Smitola, P., Hajdu, G., et al. 2015, ApJS, 219, 25
Kollmeier, J. A., Szczygieł, D. M., Burns, C. R., et al. 2013, ApJ, 775, 57
Kurucz, R. L. 2011, Canadian Journal of Physics, 89, 417
Lee, Y.-W., Demarque, P., & Zinn, R. 1990, ApJ, 350, 155
Liu, S., Zhao, G., Chen, Y.-Q., Takeda, Y., & Honda, S. 2013, Research in Astronomy and Astrophysics, 13, 1307
Marconi, M., Coppola, G., Bono, G., et al. 2015, ApJ, 808, 50
Molnár, L., Bódi, A., Pál, A., et al. 2022, ApJS, 258, 8
Molnár, L., Plachy, E., Bódi, A., et al. 2023, arXiv e-prints, arXiv:2308.01560
Molnár, L., Szabó, R., Moskalik, P. A., et al. 2015, MNRAS, 452, 4283
Morgan, S. M., Wahl, J. N., & Wieckhorst, R. M. 2007, Monthly Notices of the Royal Astronomical Society, 374, 1421
Moskalik, P., Smolec, R., Kolenberg, K., et al. 2015, MNRAS, 447, 2348
Netzel, H. 2023, arXiv e-prints, arXiv:2310.14824
Netzel, H., Molnár, L., Plachy, E., & Benkő, J. M. 2023, A&A, 677, A177
Netzel, H. & Smolec, R. 2019, MNRAS, 487, 5584
Netzel, H. & Smolec, R. 2022, MNRAS, 515, 3439
Netzel, H., Smolec, R., & Dziembowski, W. 2015a, MNRAS, 451, L25
Netzel, H., Smolec, R., & Moskalik, P. 2015b, MNRAS, 447, 1173
Netzel, H., Smolec, R., & Moskalik, P. 2015c, MNRAS, 453, 2022
Netzel, H., Smolec, R., Soszyński, I., & Udalski, A. 2018, MNRAS, 480, 1229
Paxton, B., Smolec, R., Schwab, J., et al. 2019, ApJS, 243, 10
Pietrinferni, A., Cassisi, S., Salaris, M., & Castelli, F. 2004, ApJ, 612, 168
Pietrzyński, G., Thompson, I. B., Gieren, W., et al. 2012, Nature, 484, 75
Plachy, E., Pál, A., Bódi, A., et al. 2021, ApJS, 253, 11
Rathour, R. S., Smolec, R., & Netzel, H. 2021, MNRAS, 505, 5412
Sbordone, L., Bonifacio, P., Marconi, G., Buonanno, R., & Zaggia, S. 2005, A&A, 437, 905
Smolec, R., Dziembowski, W., Moskalik, P., et al. 2017a, in European Physical Journal Web of Conferences, Vol. 152, European Physical Journal Web of Conferences, 06003
Smolec, R. & Moskalik, P. 2008, Acta Astron., 58, 233

Smolec, R., Moskalik, P., Kałużny, J., et al. 2017b, MNRAS, 467, 2349
Smolec, R. & Śniegowska, M. 2016, MNRAS, 458, 3561
Smolec, R., Ziółkowska, O., Ochalik, M., & Śniegowska, M. 2023, MNRAS, 519, 4010
Sneden, C., Preston, G. W., Kollmeier, J. A., et al. 2018, AJ, 155, 45
Soszyński, I., Poleski, R., Udalski, A., et al. 2008, Acta Astron., 58, 163
Soszyński, I., Udalski, A., Szymański, M. K., et al. 2016, Acta Astron., 66, 131
Soszyński, I., Udalski, A., Wrona, M., et al. 2019, Acta Astron., 69, 321
Süveges, M. & Anderson, R. I. 2018, MNRAS, 478, 1425
Szabó, R., Kolláth, Z., & Buchler, J. R. 2004, A&A, 425, 627
Tautvaišienė, G., Wallerstein, G., Geisler, D., Gonzalez, G., & Charbonnel, C. 2004, AJ, 127, 373
Zhang, Z., Jiang, B., Ren, Y., Chen, X., & Wang, S. 2022, ApJ, 928, 139